Corrosion analysis of stainless steel exposed to Karanja oil biodiesel: a comparative study with commercial diesel fuel, surface morphology analysis, and long-term immersion effects in alternative fuels

Q2 Q3 Q4 Q5

Maninder Singh, Mukhtiar Singh, Mandeep Singh Rayat, Ajay Sharma, Harjit Singh, Rajeev Kumar, Rajeev.14584@lpu.co.in, Shubham Sharma, https://orcid.org/0000-0001-9446-8074, shubham543sharma@gmail.com, V.K. Bupesh Raja, https://orcid.org/0000-0002-8929-1814, bupeshraja.auto@sathyabama.ac.in, Abinash Mahapatro, https://orcid.org/0000-0002-1606-8267, abinashmahapatro@soa.ac.in, Parveen Kumar, Parveen.J3181@cgcjhanjeri.in, Renu Dhiman, Deepak Gupta, deepakgupta@gehu.ac.in and Ehab El Sayed Massoud, ehabheca@kku.edu.sa

School of Mechanical Engineering, Lovely Professional University, Jalandhar, Punjab, 144001, India

Department of Technical Sciences, Western Caspian University, Baku, Azerbaijan

Centre for Research Impact and Outcome, Chitkara University Institute of Engineering and Technology, Chitkara University, Rajpura, 140401, Punjab, India

~~School of Mechanical and Automotive Engineering, Qingdao University of Technology, Qingdao, 266520, China~~

Jadara University Research Center, Jadara University, Jordan

Department of Mechanical Engineering, Sathyabama Institute of Science and Technology, Chennai, Tamil Nadu, India

Department of Mechanical Engineering, Siksha 'O' Anusandhan (Deemed to be University), Bhubaneswar, Odisha, 751030, India

Department of Mechanical Engineering, Chandigarh College of Engineering, Chandigarh Group of Colleges, Jhanjeri, Mohali, 140307, Punjab, India

School of Computer Application, Lovely Professional University, Jalandhar, Punjab, 144001, India

Department of Mechanical Engineering, Graphic Era Hill University, Dehradun, 248002, Uttarakhand, India

Department of Mechanical Engineering, Graphic Era Deemed to be University, Dehradun, Uttarakhand, 248002, India

College of Applied Sciences, Dhahran Al-Janoub, King Khalid University, Abha, Kingdom of Saudi Arabia

Corresponding authors: Rajeev Kumar, School of Mechanical Engineering, Lovely Professional University, Jalandhar, Punjab, 144001, India, E-mail: Rajeev.14584@lpu.co.in; and **Shubham Sharma**, Department of Technical Sciences, Western Caspian University, Baku, Azerbaijan; Centre for Research Impact and Outcome, Chitkara University Institute of Engineering and Technology, Chitkara University, Rajpura, 140401, Punjab, India; School of Mechanical and Automotive Engineering, Qingdao University of Technology, Qingdao, 266520, China; and Jadara University Research Center, Jadara University, Jordan, E-mail: shubham543sharma@gmail.com, shubhamsharmacsirclri@gmail.com

Abstract

The ever-growing energy demand necessitates the deployment of renewable alternatives as fossil fuel reserves diminish. The biodiesel generated from these non-edible feedstocks, such as Karanja, and Jatropha oils, offers an environmental alternative without affecting food security. Transesterification process (using methanol as solvent and sodium hydroxide (NaOH) catalyst) was used to prepare biodiesel. The stainless steel, mild steel, and cast iron materials were immersed in Karanja oil biodiesel blends (B80 and B90) and commercial diesel for 1872 h at 37 °C to critically examine the corrosion behavior with their comparison analysis. It was unveiled that biodiesel is more prone to corrosion than diesel fuel under comparable identical conditions. The corrosion rates determined by weight loss measurements in biodiesel were found to range from 0.0173 mm/year to 0.0194 mm/year for stainless steel, 0.03076 mm/year to 0.03232 mm/year for mild steel, and from 0.0505 mm/year to 0.0528 mm/year for cast iron, as compared to 0.009 mm/year for stainless steel, 0.015 mm/year for mild steel, and 0.017 mm/year respectively for cast iron in diesel. The intense severe melting of biodiesel as compared to diesel samples can be determined by employing the SEM analysis at 200X and 400X magnification scales. Hence, this study has underscored the significance of selecting the appropriate corrosion resistant materials that are suitable for the continued prolonged storage and utilization or application biodiesel.

Keywords Karanja oil; *trans*-esterification; corrosion; stainless steel

Abbreviations

FAME Fatty acid methyl esters

FAEE Fatty acid ethyl esters

AISI American Iron and Steel Institute

ASTM American Society for Testing and Materials

TAN Total acid number

EIS Electrochemical Impedance Spectroscopy

GC Gas Chromatography

MS Mass Spectrometry

SEM Scanning Electron Microscopy

1 Introduction

Industrialization and increase in demand of energy consumption increased interest in alternative fuels resources of resources of petrochemical fuels. Biodiesel is alternative for conventional petrochemical fuels. Biodiesel can be produced from various edible and non-edible feedstocks. Focus was made on non-edible feedstocks for production of biodiesel [1]. Since biodiesel and diesel fuel are fully miscible, they can be combined in varying proportions that are already used in a number of countries. The US uses blends, B5 – B20, Indonesia uses mainly B20, Brazil uses B11, Argentina uses B10, Germany uses blends of between B5 – B7. 5. They are a viable, promising alternative energy source [2], [3]. Four non-edible resources such as Neem, Karanja, jatropha and rubber were studied due to their multipurpose use. They can be used for medicine, fuel, dyes, soil enrichment etc. They can be also grown in diverse environmental conditions. Jatropha was used in insecticide and pesticides also [4]. Alternative fuels (for example ammonia, hydrogen, methanol, methane and biofuel) are one option for reducing the carbon emissions in order to avoid dependence on fossil fuels. One of these is hydrogen, a non-toxic, odourless and renewable energy. Its carbon-empty combustion yields nothing but water making it clean fuel, and fittingly, researchers have been

studying hydrogen applications. [5]. Variety of homogenous and heterogeneous catalytic transesterification processes were used for biodiesel production. Due to cutting edge advancements Enzyme catalyzed transesterification was used for the production of biodiesel from animal fat [6]. Animal bone was also used as catalyst for production of biodiesel. Animal bone was having advantage of remaining active even after multiple transesterifications [7]. High cetane number, non-toxic nature and non-availability of Sulfur content makes biodiesel most appropriate alternative fuel. But the storage stability of biodiesel is major concern due to presence of unsaturated methyl esters component. The rate of degradation during storage increased with unsaturated methyl ester component. Degradation of fuel properties was also enhanced with sunlight and direct air contact. The automotive engine characteristics were also affected due to fuel properties degradation by long term storage [8]. A leading cause of failure in a fuel storage tank is corrosion (moderate-to-severe corrosion found in over 80% of tank systems). This common issue results in massive maintenance expenses, costing billions of dollars a year to fix and replace them [9]. Corrosion removes metal ions from surface. These metal ions enhance oxidation of biodiesel leading to composition and quality change of fuel. However, presence of FAME and FAEE shows little effect on AISI stainless steel degradation [10]. When biodiesel oxidizes, it degrades and produces by products that can pollute the fuel. Everyone knows biodiesel is more corrosive than regular Petro diesel [11]. GS, CS, and SS storage tanks were exposed to palm-in-EDB 7 months, and the study investigates their individual corrosion behaviour. Localized corrosion was observed for SS tanks and generalized corrosion for GS and CS tanks, with maximum leak potential at tank base. For instance, the results of this study also indicate that SS tanks showed lower oil contamination, which highlights the importance of material selection when storing biodiesel [12]. Biodiesel derived from different resources have different amount of unsaturated methyl esters. Oxidation reactions on exposure of air and light can change into long chain fatty acid. This can affect the performance of biodiesel in diesel engine. The neutralized soybean oil-based biodiesel shoes more oxidation stability due to presence of naturally present antioxidants. On other hand degradation of antioxidants due to heating reduces oxidation stability of frying oil waste-based biodiesel [13]. In light metals magnesium was comparatively corroded more than aluminum by palm oil biodiesel. Weight loss measurement clearly indicates corrosion after being placed in palm oil biodiesel for 1,440 h. A gel like sticky mass covered surface of magnesium after exposure with biodiesel [14]. Corrosive behavior of ASTM 1045 mild steel was studied by static immersion test for 30, 60 and 120 days in palm biodiesel. Results showed that palm biodiesel was more corrosive compared to diesel. Temperature range of 27, 50 and 80 was used for static immersion test. Exposure time and temperature also have important role in corrosion [15]. The growing use of biodiesel in the transportation sector has sparked concerns regarding its corrosive effect on engine and fuel system materials. Studies on rapeseed oil biodiesel-diesel blends (B0–B100) show that copper and brass showed very high corrosion susceptibility, 5 and 3.5 times higher than the rate in diesel, respectively. On the other hand, aluminium, zinc and stainless-steel exhibit high resistance to corrosion and negligible deterioration. Increasing biodiesel fractions caused a focussed mode of attack and a much higher degree of acid formation, while low blends showed good performance in preventing degradation and acidity development [16]. Weight loss measurement after static immersion and potentiostat electrochemical techniques to find effect of corrosion on engine parts. Stainless steel possesses least corrosion compared to specimen of aluminum, copper, copper alloys and elastomers. Surface morphology revealed type of corrosion and nature of occurrence. Auto-oxidation and presence of moisture were the main reasons of degradation. A new phase was formed in specimen when exposed to biodiesel blends as revealed by X-ray diffractometer [17]. The corrosion behaviour of stainless steels was examined in soybean-based biodiesel, taking into account differences in material structures (austenitic, ferritic and austenitic-ferritic) and compositions. The potentiodynamic polarization and weight loss tests, as well as the optical microscopy, were used to test AISI 304L, Sea Cure and Duplex 2,205 stainless steels. Results showed very low corrosion rates for all materials tested, with Duplex 2,205 displaying the highest corrosion resistance and nobler potential, while Sea Cure had the lowest resistance values according to EIS studies. The results indicate that all three stainless steels are appropriate for biodiesel applications [18]. Measuring electrochemical noises was another innovative technique used for determination of corrosion on engine parts under different working conditions. Explaining start of corrosion and drawing conclusion of its development with time makes this process advantageous over standardized method for corrosion testing i.e. Salt-spray testing, electrochemical polarization [19]. Electrochemical testing technique was used to determine corrosive behavior of aluminum. Results demonstrated similarity of corrosion of aluminums in alkali contaminated biodiesel with the same sample in aqueous solution [20]. Stainless steel and tin exhibited good resistance to corrosion in bioethanol and its blends, while copper and carbon steel are very sensitive to this type of corrosion. The least corroded material observed was tin, with stainless steel being second. The more ethanol is present, the more the materials corrode. Biofuels are less common for carbon steel and copper, and more appropriate for stainless steel and tin [21]. In this study, the static immersion and vapor phase tests at 50 °C for 2,160 h were used to evaluate the corrosion behaviour of carbon steel, stainless steel, aluminum as well as copper in biodiesel-Petro diesel blends. Copper displayed the maximum corrosion rates in B7 blend, 9.5273 μm/y (partial), 9.1484 μm/y (total), and 6.6178 μm/y (crevice) and the minimum corrosion in B15 and B30 blends. Minimal surface changes were observed for carbon steel and stainless steel however in the vapour phase carbon steel corroded. Aluminum showed good compatibility with no corrosion or surface compound formation. Copper was found to be the most influencing component on the oxidative stability of biodiesel [22]. Static immersion test at room temperature and 60 °C was used to study corrosion behavior. Surface morphology of corrosion products and chemical structure revealed lower corrosion in B20D70E10 than neat biodiesel. Pure petro-diesel has least corrosion and degradation of fuel properties. Acid concentration is measured in terms of TAN (Total acid number) in non-aqueous solution. The TAN value of B20D70E10 upon exposure to carbon steel exceeds than the limit as per ASTM Standard (0.8 mg of KOH/g). The TAN no increases with increase in products of oxidation representing enhancement in corrosion due presence of excessive corrosive acids [23]. Corrosion rate of copper and aluminum in Biodiesel was high compared to rather than stainless steel. Rise in temperature, content of water and oxides also enhanced corrosion rate [24].

Previous studies investigating the corrosive properties of biodiesel in comparison to standard diesel fuel found the saturated methyl esters and oxidation by-products in biodiesel to induce degradation of materials, leading to fouling and performance issues. Although there is a considerable amount of literature available for the corrosion behavior of metals (such as stainless steel, carbon steel, aluminum, and copper) in biodiesel, very limited literature is available regarding biodiesel produced from non-edible feedstocks, such as Jatropha and Karanja oils. n the case of use of these biodiesel blends, it has been observed that the corresponding corrosion behavior of materials has not been sufficiently studied. Stainless steel is more corrosion resistant than copper or carbon steel in biodiesel (especially at higher concentration) according to many studies. However, the long-term corrosion data of metals exposed to biodiesel from non-edible sources is still scare, and factors like storage conditions are seldom discussed. This research seeks to address these gaps by studying the corrosion behavior of stainless steel, mild steel, and cast iron in Karanja oil biodiesel blends (B80 and B90) and comparing the same with commercial diesel. Experimental design: Metal samples are submerged in biodiesel at 37 °C for a duration of 1,872 h; corrosion rates are calculated based on weight loss measurements, and surface morphology is demonstrated through optical microscopy at 200X and 400X magnifications. The study will provide fundamental information for materials selection in biodiesel storage and transportation systems, particularly for biodiesel produced from non-edible oil sources such as Karanja and Jatropha oils. Figure 1 has depicted the Flow chart of process methodology.

Figure 1:

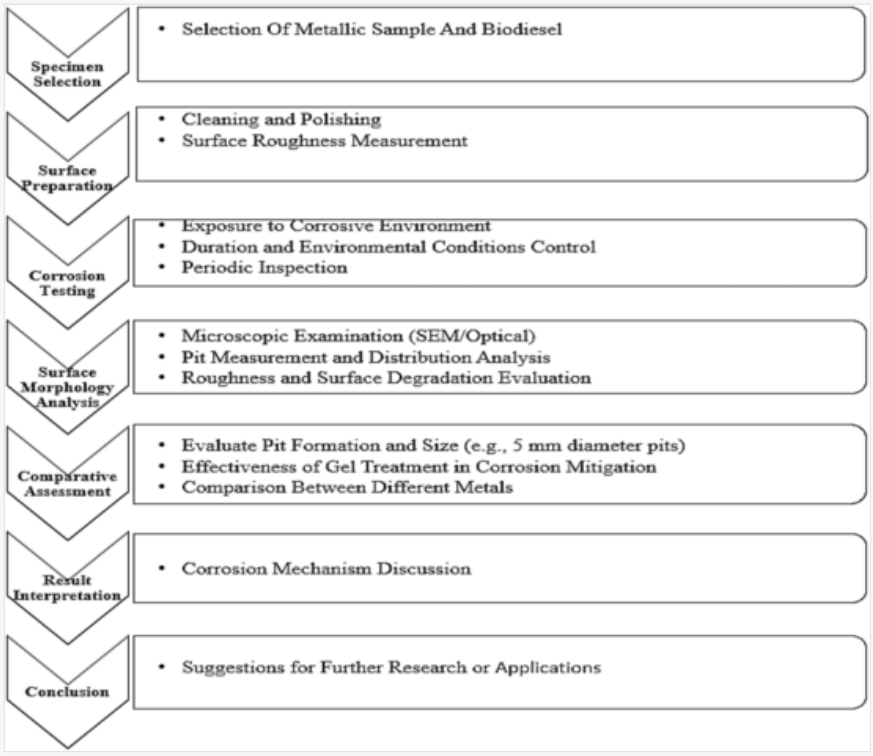

Flow chart of process methodology.

2 Experimental process

2.1 Materials and methodology

Q6 Karanja and Jatropha oils were used as feedstocks to produce biodiesel [28]. Transesterification process using methanol as the alcohol and sodium hydroxide (NaOH) as the catalyst. The in-cube corrosion assessment was performed using two biodiesel blends, namely B80 (80% biodiesel, by volume) and B90 (90% biodiesel, by volume). Parts with total dimensions of 46 mm × 46 mm × 2 mm of stainless steel and cast-iron were prepared to evaluate the corrosion. These materials were selected to study the effect of different biodiesel blends on the corrosion resistance of different metals. Microstructure of the specimens (prior to corrosion test) was investigated at various magnification levels to record surface variations. The images at 200X and 400X magnifications for mild steel, stainless steel and cast iron are shown in Figure 2(a–f) detailing the surface structure of the materials.

Figure 2:

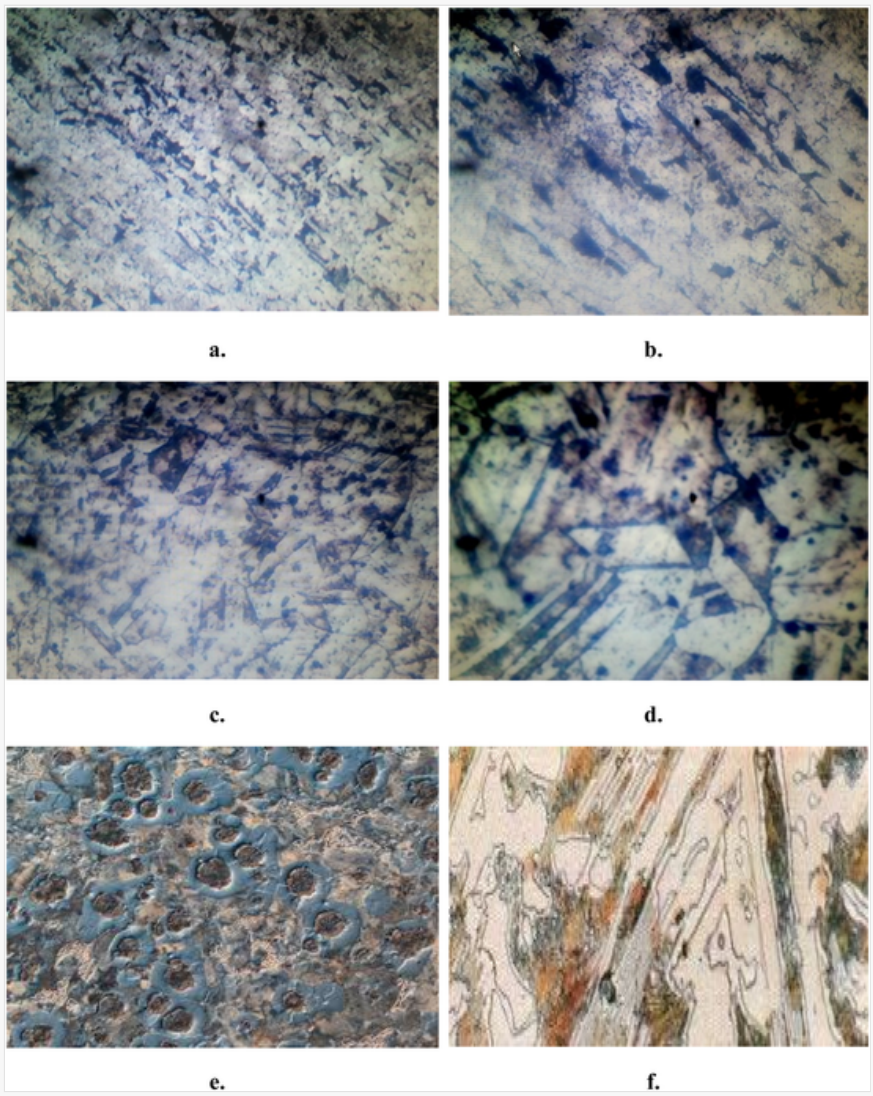

Specimens surface structure under different magnifications (a) Mild steel 200X (b) Mild steel 400X (c) Stainless steel 200X (d) Stainless steel 400X (e) Cast iron 200X (f) Cast iron 400X.

Surface of mild steel, stainless steel, and cast iron at different magnifications Mild steel at 200X shows a fairly homogenous single-particle structure with visible ferrite and pearlite phases whereas at 400X, individual particles and finer detail like particle boundaries can be seen. Stainless steel, with a high corrosion resistance comes very

homogenously at 200X, the austenitic and ferritic mixture can be seen, as well as the detail at 400X, where you can see some crystalline structuring and boundaries. In contrast, cast iron has a less homogenous structure due to the presence of graphite flakes or nodules; and the distribution of these graphite structures within the iron matrix can be viewed at 200X, while at 400X, the size, shape and distribution of the graphite morphology becomes apparent. In general, magnification plays a big role in determining whether or not microstructural features can be seen, with low levels providing an overview and higher levels revealing details fundamental to understanding the material.

2.2 Transesterification route for synthesis of bio-diesel

The transesterification process is an established chemical method for converting triglycerides into fatty acid methyl esters (FAME) through the reaction with an alcohol, typically methanol, in the presence of a catalyst. Transesterification starts with several steps: (i) the triglycerides used are converted into diglycerides and monoglycerides and broken down, (ii) free fatty acids present in the feedstock react to neutralize the process, preventing soaps which must form; (iii) after the production of the by-product-glycerol which must also be separated away and (iv) the formation of the product, methyl esters (biodiesel). After completion of the reaction, the mixture gradually cooled to promote phase separation. The heavier glycerol by-product sank to the bottom and was carefully siphoned off. The upper biodiesel layer rich in FAME were washed with water to eliminate residual alcohol, catalyst, and impurities to obtain biodiesel that meets fuel standards. Different feedstocks used for producing biodiesel were analysed for their physiochemical properties to determine its potential use as alternate fuel. The key physiochemical characteristics of Karanja biodiesel are shown in Table 1, including density, viscosity, flash point, and cetane number. Also shown in Table 2 is a comparison of the properties of Jatropha biodiesel which pinned down the quality of the fuel based on feedstock.

Table 1:

Properties of Karanja biodiesel.

Property (Unit)	Karanja biodiesel (B80)	Std limits	
		diesel	biodiesel
Flash point (°C)	148.3	67	≥130
Moisture content % (v/v)	0.03 %	Max. 0.02 %	Max. 0.05 %
Cloud point (°C)	6	–	–
Pour point (°C)	3	3 °C winter & 15 summer	
Total sulphur (ppm)		350 Max	
Calorific value (KJ/Kg)	36,871		
Density (g/cm^3) at 15 °C	0.892	0.820–0.860	0.880–0.890
Kinematic viscosity (mm^2/s) at 40 °C	4.92	2.00–5.00	1.90–6.00
Oxidation stability (IP, at 140 °C,hr)	2.98		3 h (min), 6 h (min)
Appearance	Slight yellowish	Light red	–
Acidity/mg KOH g^{-1}	0.224	0.4836	≤0.5
Distillation temperature (50 %)/°C	283	275	≤360
Mechanical impurities (m/m)/%	No	No	No

Table 2:

Property of Jatropha biodiesel.

property (unit)	Jatropha biodiesel	Std limits	
		Diesel	Biodiesel
Flash point (°C)	134	67	≥130
Moisture content % (v/v)	0.00 %	Max. 0.02 %	Max. 0.05 %
Cloud point (°C)	3	–	–
Pour Point (°C)	−3	3 °C winter & 15 summer	
Total sulphur (ppm)	336 Max	350 Max	
Calorific value (KJ/Kg)	43,358		
Density (g/cm^3) at 15 °C	0.8309	0.820–0.860	0.880–0.890
Kinematic viscosity (mm^2/s) at 40 °C	3.07	2.00–5.00	1.90–6.00
Oxidation stability (IP, at 140 °C, h)	2.98		3 h (min), 6 h (min)
Appearance	Light yellowish	Light red	–
Acidity/mg KOH g^{-1}	0.2244	0.4836	≤0.5
Distillation temperature (50 %)/°C	287	275	≤360
Mechanical impurities (m/m)/%	No	No	No

2.3 Corrosion analysis

The test conditions for corrosion were based on the ASTM G32-72 (Laboratory Immersion Corrosion Testing of Metal); room temperature was selected to represent a typical environment for metals in biodiesel and diesel fuels. They were immerged in a plastic beaker containing biodiesel and their initial weights (m_1) were recorded. Before testing, the metal surfaces were scrupulously cleaned with acetone and polished with silicon carbide paper to remove contaminants and ensure a smooth and uniform

surface. Such preparation was important to limit the role of surface contaminants in corrosion. A controlled experimental design with three groups of nine tubes each was used in this study. In the first part of the experiment, strips of cast iron, mild-steel and stainless-steel were placed into separate tubes each containing 100 g of biodiesel to ensure that the metals were completely immersed. The second group performed the same process as above, except for the testing fluid, which was regular diesel rather than the biodiesel. This enabled direct comparison of the impact of biodiesel and diesel on the corrosion rates of the metals. All the metals were detached weekly after immersion and cleaned with acetone to remove impurities from their surfaces. Then a hairdryer was used to dry the metals as any external moisture could affect measurements. Their weight was then documented as m_2 and corrosion rates were determined by using the following equation:

$$K_L = \frac{(m_2 - m_1) \times 24 \times 365}{\rho^{TS \times 1000}} = 8.76 \times \frac{\Delta \boldsymbol{m}}{\rho TS} \quad (1)$$

where, T: corrosion duration, h; S: metal area of corrosion which was from the exposed metal block (L mm × B mm × H mm), m_2. m_1: weight before corrosion, g; m_2: weight after corrosion, g; KL: corrosion rate, mm/year; Δm: metal quality change, g; ρ: metal density, g/cm^3. A caliper with a precision of 0.02 mm was used to measure the metal blocks' length, breadth, and height.

The dimensions of the metal blocks were measured using a calliper accurate to 0.02 mm to calculate the surface area accurately. The immersion test samples were prepared with appropriate dimension for each metal, (D = 13 mm, H = 49 mm) for cast iron, (46 mm × 46 mm × 2 mm) for mild steel and (36 mm × 9 mm × 9 mm) for stainless steel. For Cast iron the surface area was 1,458 mm^2. This was found to be 4,600 mm^2 for the mild steel specimen. The surface area for the stainless steel specimen was proper at 1,858.25 mm^2. Such surface area values play an important role in terms of obtaining the corrosion rate since they are the area of each specimen exposed to biodiesel or diesel in the immersion tests. These Specimens were mechanically polished using abrasive paper from 220 to 1,000 grit to a uniform surface finish. The Specimens were then suspended in beakers containing 100 g of biodiesel (in triplicates). For the static immersion test, the Specimens were tied with silk string so that the Configurations could maximize the area of the metal surface exposed to the fluid. The Specimens were rinsed with acetone and accurately weighed with an electric scale (accuracy to 0.01 mg) before immersion. As shown in Figure 3(a–f), three metal samples used are: mild steel, stainless steel, cast iron and these were dipped separately in three beakers containing diesel and papered 2 biodiesels separately as exhibited in the Figure 3(a–f). A small plastic box was placed over each beaker to avoid contamination by external debris and maintain a controlled testing environment for the duration of the experiment. Tests were performed at room temperature over the course of 1,872 h. After the immersion time ended, all Specimens were cleaned with a soft toothbrush to remove corrosion products and were rinsed in deionized water. The metals were degreased with acetone prior to final weight measurement. This cleaning process was critical for accurately measuring weight loss during the corrosion test and, consequently, calculating the actual corrosion rate.

Figure alignment: The figure layout displayed in this section is not how it will appear in the final version. As per journal style, figures will only be left aligned. The presentation below is for the sole purpose of providing corrections to the figures. To view the actual presentation of the figures, please click on the PDF located at the top of the page.

Figure 3:

Q7 Fig.3 ~~(a–f)~~. (a-e). Samples and specimens and (f). weight measuring device.

2.4 Weight reduction method

In the present study, non-consumable biodiesel samples including Karanja and Jatropha biodiesel and ferrous metal specimens including low carbon steel and stainless steel were studied for their corrosion behaviour. The samples were immersed for 1,822 h, and major mass and other property changes were monitored throughout the immersion. Biodiesel samples were poured into cylindrical beakers into which strips of ferrous material was submerged completely. During the testing period, loss of mass, as well as other physical property transformations were detected over the storage time of the metal samples.

In order to mimic the corrosion, static immersion testing was carried out in accordance with (ASTM G32-72). Cylindrical beakers held biodiesel samples, while Specimens of workpiece material were soaked for a period of 1,872 h. The weight loss due to the release of metal from the surface, along with variations in other materials properties, act as corrosion diagnostic during this period. The details of the degradation were carefully quantified over time to capture both the rate and mechanism of material degradation. Surface finishing of the metal Specimens was performed with sandpapers having various grits (200, 600 and 1,000) after power wheel grinding. The polishing was done with a 0.6-μm diamond paste for a smoother finish. The samples were also etched with 98% methanol and 2% nitric acid solution and washed with normal water to remove residual chemicals. After cleaning and drying, the weight of each sample was accurately measured using an electronic balance with 0.01 mg precision. Corrosion rate was calculated by the following equation [24], [25].

$$v_{\text{corr}} = \frac{(m_2 - m_1) \times 24 \times 365}{\rho TS} \quad (2)$$

where $v_{\text{corr:}}$ corrosion rate (mm/year), m_1: Weight of initial sample (grams), m_2: Weight after corrosion, T: corrosion time, S: Surface area of work piece and ρ: workpiece density. The experimental setup is shown in Figure 4.

Figure 4:

Experimental procedure.

3 Results and discussions

3.1 Analysis of fatty acid composition modifications

The analysis of methyl and ethyl esters in biodiesel samples at various stages of oxidation was carried out by gas chromatography (GC) hyphenated to mass spectrometry (MS). The sample was transported from the injector to the gas chromatograph by an inert gas, serving as the mobile phase. When ionization processes sent the molecules toward the mass spectrometer, those with lower boiling points travelled faster. Identifying individual components in the sample was performed by comparing the obtained data with a standard library. Analytical sample preparation included the filtration of the sample through a 0.45 μm filter to remove any particulate matter, as described previously. The injector was maintained at 250 °C and was injected with 0.1 μl of the sample biodiesel, which was carried through 1.5 mL/min of inert gas. In that case, for the corrosion test exposure time was plotted against the corrosion rate (mm/year) to observe a correlation. The three test samples were two biodiesels (Karanja and Jatropha) and a commercial diesel. The test samples were made from cast iron, mild steel, and stainless steel. Corrosion rate for each sample was calculated with the formula described earlier. The pre-corrosion weight (m_1 in grams), post-corrosion weight (m_2 in grams), corrosion rate (KL in mm/year), metal qualitative change (Δm in grams), metal density (ρ in g/cm^3), corrosion time duration (T in hours), and metal area of corrosion (L mm × B mm × H mm) were noted. The sizes of metal blocks were accurately measured with a calliper with an accuracy of 0.02 mm. The surface area on the specimen that had been exposed to biodiesel was calculated based on its dimensions and included in the analysis was the exposition time. Table 3 shows the recorded data according to the weight variation with time for each of the specimen exposed to biodiesel or commercial diesel during the overall testing period. The differences in the corrosiveness of the three fuels and the practical importance of the data were evident, and corroborate similar findings previously published, though these measurements are the first of their kind in pure biodiesel environments.

Table 3:

Variation in weight of specimen with time.

Specimens →		Cast iron	Mild steel	Stainless steel	Cast iron	Mild steel	Stainless steel/b90(j)	Cast iron	Mild steel	Stainless steel
Samples →		Diesel	Diesel	Diesel	B90(J)	B90(J)	B90(J)	B80(K)	B80(K)	B80(K)
Dimensions (mm)		36 × 9 × 9	46 × 46 × 2	D = 13 H = 49	36 × 9 × 9	46 × 46 × 2	D = 13 H = 49	36 × 9 × 9	46 × 46 × 2	D = 13 H = 49
Surface area (mm^2)										
Original wt (m_1) (gm)		34.16	71.66	79.6	33.81	72.12	78.06	33.82	71.74	78.87
Total weight		97.3	174.04	152.56	84.16	169.71	158.97	83.84	155.13	143.28
Hours ↓	Date ↓									
0 HRS	5-Feb	34.16	71.66	79.6	33.81	72.12	78.06	33.82	71.74	78.87
72 HRS	8-Feb	34.12	71.66	79.6	33.8	72.11	78.06	33.8	71.73	78.87
144 HRS	11-Feb	34.11	71.64	79.6	33.75	72.1	78.05	33.76	71.71	78.86
216 HRS	14-Feb	34.09	71.64	79.59	33.7	72.05	78.05	33.74	71.71	78.86
288 HRS	17-Feb	34.07	71.63	79.55	33.65	72	78.04	33.68	71.69	78.85
360 HRS	20-Feb	34.06	71.63	79.5	33.58	71.98	78.04	33.64	71.69	78.85
432 HRS	23-Feb	34.03	71.62	79.49	33.52	71.97	78.02	33.61	71.67	78.83
504 HRS	26-Feb	34.01	71.6	79.49	33.48	71.95	78.02	33.57	71.63	78.82
576 HRS	29-Feb	33.96	71.54	79.46	33.42	71.9	77.98	33.52	71.58	78.79

648 HRS	3-Mar	33.91	71.52	79.46	33.4	71.88	77.98	33.49	71.57	78.79
720 HRS	6-Mar	33.85	71.47	79.43	33.37	71.87	77.97	33.42	71.55	78.75
792 HRS	9-Mar	33.81	71.43	79.43	33.32	71.87	77.96	33.39	71.53	78.75
864 HRS	12-Mar	33.77	71.41	79.41	33.28	71.85	77.94	33.35	71.5	78.72
936 HRS	15-Mar	33.69	71.39	79.41	33.25	71.8	77.94	33.31	71.47	78.72
1,008 HRS	18-Mar	33.62	71.35	79.38	33.2	71.79	77.92	33.28	71.45	78.7
1,080 HRS	21-Mar	33.56	71.33	79.37	33.17	71.74	77.91	33.24	71.41	78.69
1,152 HRS	24-Mar	33.51	71.29	79.37	33.13	71.73	77.89	33.21	71.39	78.69
1,224 HRS	27-Mar	33.43	71.26	79.33	33.11	71.73	77.89	33.17	71.37	78.67
1,296 HRS	30-Mar	33.39	71.24	79.32	33.08	71.71	77.86	33.13	71.34	78.66
1,368 HRS	2-Apr	33.35	71.22	79.32	33.04	71.69	77.85	33.09	71.31	78.65
1,440 HRS	5-Apr	33.31	71.19	79.3	32.98	71.65	77.84	33.07	71.28	78.64
1,512 HRS	8-Apr	33.27	71.16	79.29	32.93	71.62	77.82	33.01	71.25	78.62
1,584 HRS	11-Apr	33.22	71.14	79.27	32.87	71.58	77.79	32.95	71.21	78.59
1,656 HRS	14-Apr	33.18	71.11	79.26	32.83	71.56	77.76	32.91	71.21	78.54
1,728 HRS	17-Apr	33.14	71.11	79.24	32.8	71.54	77.74	32.78	71.19	78.53
1,800 HRS	20-Apr	33.11	71.08	79.24	32.77	71.52	77.73	32.75	71.16	78.52
1,872 HRS	23-Apr	33.09	71.07	79.21	32.73	71.52	77.72	32.71	71.15	78.51

Table 4 has illustrated the corrosion rate computation of different specimen in Diesel/Jatropha/Karanja.

Table 4:

The table layout displayed in this section is not how it will appear in the final version. The representation below is solely purposed for providing corrections to the table. To view the actual presentation of the table, please click on the PDF located at the top of the page.

Corrosion rate for specimens in Diesel/Jatropha/Karanja.

Specimen	Formula	Diesel/Jatropha/Karanja	Diesel/Jatropha/Karanja
Corrosion rate of cast iron	$K_L = \frac{(m_2 - m_1)\times 24\times 365}{\rho TS\times 1000} = 8.76\times\frac{\Delta m}{\rho TS}$	$K_L = 8.76\times\frac{1.07}{185.59}$, $K_L = 8.76\times\frac{1.09}{185.59}$, $K_L = 8.76\times\frac{1.12}{185.59}$,	0.0505 mm/year 0.0514 mm/year 0.0528 mm/year
Corrosion rate of mild steel	$K_L = \frac{(m_2 - m_1)\times 24\times 365}{\rho TS\times 1000} = 8.76\times\frac{\Delta m}{\rho TS}$	$K_L = 8.76\times\frac{0.59}{168.02}$, $K_L = 8.76\times\frac{0.6}{168.02}$ $K_L = 8.76\times\frac{0.62}{168.02}$	0.03076 mm/year 0.03128 mm/year 0.03232 mm/year
Corrosion rate of stainless steel	$K_L = \frac{(m_2 - m_1)\times 24\times 365}{\rho TS\times 1000} = 8.76\times\frac{\Delta m}{\rho TS}$	$K_L = 8.76\times\frac{0.33}{166.410}$ $K_L = 8.76\times\frac{0.34}{166.410}$ $K_L = 8.76\times\frac{0.37}{166.410}$	0.0173 mm/year 0.0178 mm/year 0.0194 mm/year

The corrosion rates of cast iron specimens exposed to diesel, Jatropha and Karanja are shown in Figure 5. The corrosion rates calculated for diesel, 0.0505 mm/mm/year, 0.0514 mm/year 0, 00.0454mm 00.0514 for Jatropha and 0.0528 mm/year for Karanja. These results show that Karanja is the most corrosive, followed by Jatropha and diesel. The data show that different fuels have varying corrosive effects on cast iron, and underscore the importance of careful material selection when using this metal.

Figure alignment: The figure layout displayed in this section is not how it will appear in the final version. As per journal style, figures will only be left aligned. The presentation below is for the sole purpose of providing corrections to the figures. To view the actual presentation of the figures, please click on the PDF located at the top of the page.

Figure 5:

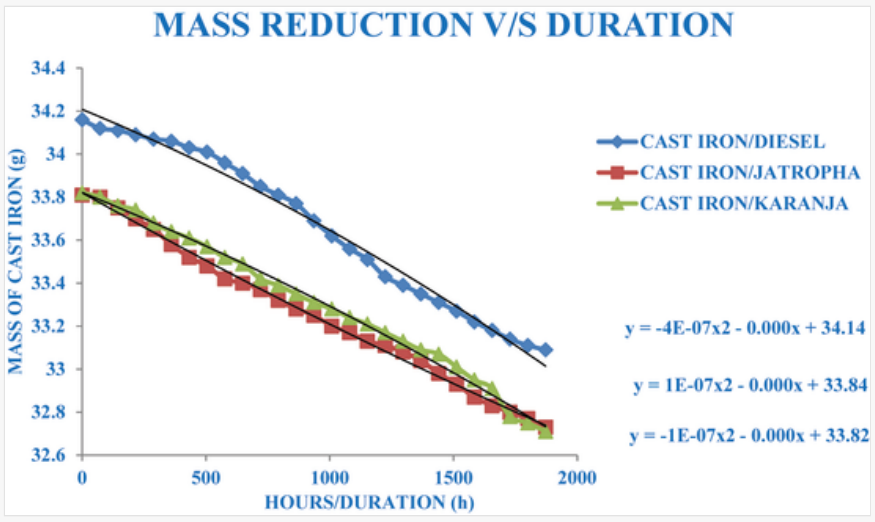

Graph of mass reduction v/s storage time of cast iron.

Corrosion rates for mild steel exposed to the same fuels are shown in Figure 6. The calcium corrosion rates are 0.03076 mm/year for diesel, 0.03128 mm/year for Jatropha and 0.03232 mm/year for Karanja. Specifically, Karanja appears to have the largest corrosion rates once again, indicating a more aggressive corrosive act than other fuels. Gradually diesel was shown to be the least corrosive leaving it with the potential to prolong the other applications, mild steel components working life.

Figure alignment: The figure layout displayed in this section is not how it will appear in the final version. As per journal style, figures will only be left aligned. The presentation below is for the sole purpose of providing corrections to the figures. To view the actual presentation of the figures, please click on the PDF located at the top of the page.

Figure 6:

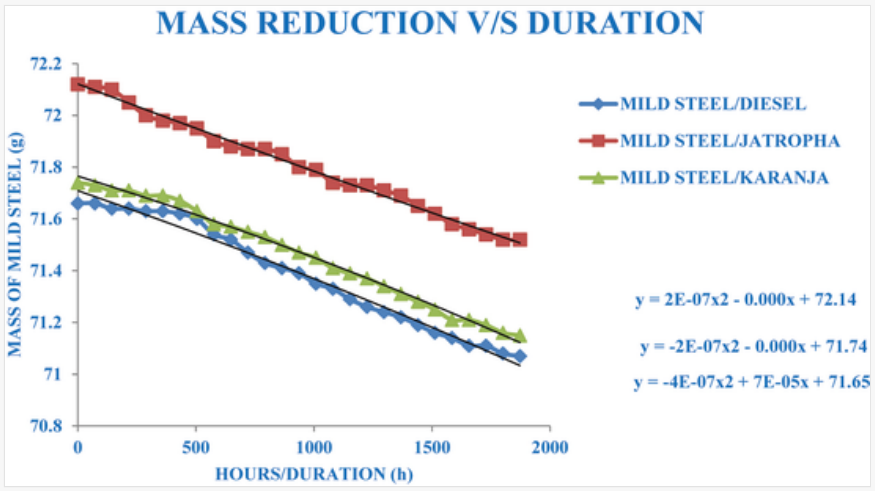

Graph of mass reduction v/s storage time of mild steel.

The corrosion rates of stainless steel in diesel, Jatropha, and Karanja are presented in Figure 7. So, the estimated data read the corrosion rates to be 0.0173/year for diesel, 0.0178 mm/year for Jatropha and, 0.0194 mm/year for Karanja. Specifically, we found that the lowest corrosion rates of the three materials examined are associated with stainless steel, which can be interpreted as a higher resistance to corrosion. Although they corrode faster than diesel, Karanja shows a more favourable regime than cast iron and mild steel and strengthens the argument to consider stainless steel in a corrosive environment.

Figure alignment: The figure layout displayed in this section is not how it will appear in the final version. As per journal style, figures will only be left aligned. The presentation below is for the sole purpose of providing corrections to the figures. To view the actual presentation of the figures, please click on the PDF located at the top of the page.

Figure 7:

Graph of mass reduction v/s storage time of stainless steel.

Corrosion rates for a variety of metals exposed to biodiesel are evidenced in Figure 8 exhibiting differences in corrosion rates among cast iron, mild steel and stainless steel. Among all the materials considered, cast iron showed the highest corrosion rate with Karanja biodiesel, suggesting that it is susceptible to corrosion in aggressive environments. Mild steel exhibited marginally lower corrosion rates compared to cast iron with an identical trend of enhanced degradation in presence of biodiesels Karanja and Jatropha. Whereas stainless steel also showed the lowest corrosion rates overall, indicating its greater corrosion resistance than the other two metals. Although the corrosion rates of all metals increased when we added Karanja, the increase on the stainless steel was relatively much smaller. In studies involving biodiesel these results are critical, as they demonstrate that stainless steels appear to resist corrosion considerably better than alternatives, as well as mitigating maintenance and replacement costs in a corrosive environment.

Figure alignment: The figure layout displayed in this section is not how it will appear in the final version. As per journal style, figures will only be left aligned. The presentation below is for the sole purpose of providing corrections to the figures. To view the actual presentation of the figures, please click on the PDF located at the top of the page.

Figure 8:

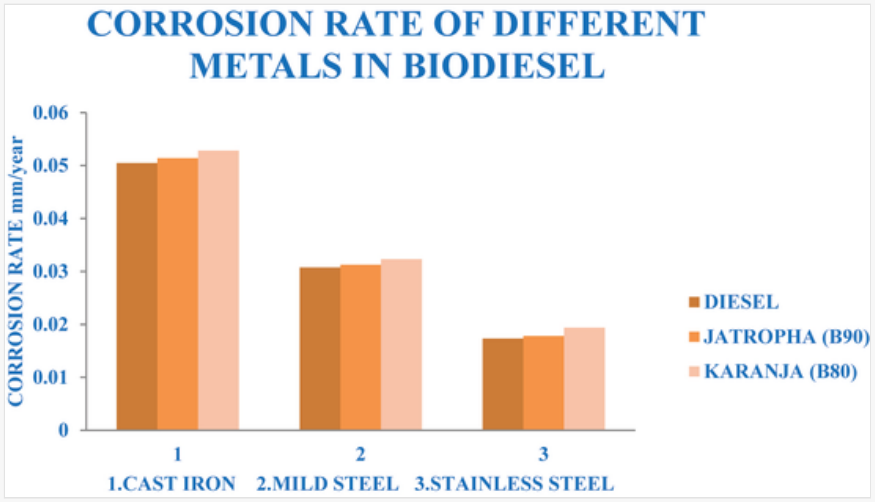

Corrosion rate of different metals in biodiesel.

3.2 Given value of specimen

Table 5 has depicted the given parameters.

Table 5:

The table layout displayed in this section is not how it will appear in the final version. The representation below is solely purposed for providing corrections to the table. To view the actual presentation of the table, please click on the PDF located at the top of the page.

Given parameters.

Specimens	Δm (g)	ρ (g/cm^3)	S (mm^2)	T (h)
Cast iron	1.07, 1.09, 1.12	6.8	1,458	1,872
Mild steel	059, 0.60, 0.62	7.85	4,600	1,872
Stainless steel	0.33, 0.34, 0.37	7.88	1,858.25	1,872

3.3 Chromatography results of Jatropha and Karanja

Jatropha and Karanja biodiesel chromatography results shows the differences in their fatty acids composition that affect their fuel properties. Table 6 and Table 7 has exhibited the chromatography result of Jatropha and Karanja.

Table 6:

The table layout displayed in this section is not how it will appear in the final version. The representation below is solely purposed for providing corrections to the table. To view the actual presentation of the table, please click on the PDF located at the top of the page.

Chromatography result of Jatropha.

Fatty acid methyl esters	CN/DB abbreviations	Wt.%
Lauric	C12:0	0.0
Myristic	C14:0	0.2
Palmitoleic	C16:1	1.0
Palmitic	C16:0	12.6
Linoleic	C18:3	4.6
Linolenic	C18:2	46.3
Oleic	C18:1	28.5
Stearic	C18:0	4.1
Eicosane	C20:1	0.4
Arachidic	C20:0	0.2
Arachidonic	C22:1	0.1
Behenic	C22:0	0.3
Nervonic	C24:1	0.1
Lignoceric	C24:0	0.0
Saturated	–	18.02
Unsaturated	–	81.9

Table 7:

The table layout displayed in this section is not how it will appear in the final version. The representation below is solely purposed for providing corrections to the table. To view the actual presentation of the table, please click on the PDF located at the top of the page.

Chromatography result of Karanja.

Fatty acid methyl esters	CN/DB abbreviations	MB (wt %)

Palmitic	C16:0	11.0 ± 0.1
Stearic	C18:0	3.5 ± 0.2
Oleic	C18:1	23.4 ± 0.3
Linoleic	C18:2	54.0 ± 0.2
Linolenic	C18:3	6.4 ± 0.1
Others	–	1.2
Saturated	–	15.2
Unsaturated	–	84.5

Jatropha biodiesel has a high percentage of unsaturated fatty acids, where Linolenic acid (C18:2) is 46.3% and Oleic acid (C18:1) is 28.5%, with a moderately high unsaturation ratio of 81.9%. Unlike Karanja, Linoleic acid (C18:2) is one of the highest in the Jatropha oil, at 54.0%, the unsaturation degree is 84.5%, contrary to Jatropha. The Phytochemical analysis of the seed oils depicted a small amount of saturated fatty acids in both the biodiesels at a range of least 12.6% in Jatropha and 11.0% in Karanja which is the dominant one in Jatropha and Karanja, respectively. Jatropha is also characterized by significant levels of Stearic acid (C18:0) and Linolenic acid (C18:3), which contribute to the overall variety of its fatty acid profile. This high unsaturation of both fuels also suggests better combustion properties and lower viscosity, but may also make them more susceptible to oxidation and material degradation. We expect that the fuel properties of the biodiesels would be similar based on the biodiesel fatty acid profiles despite the somewhat higher unsaturation of Karanja biodiesel which may influence its oxidative stability and long-term storage behavior.

3.4 Surface morphology of specimen

The surface morphology analysis of corroded metal specimens illustrates in Figure 9(a–e) show that different material types and protective treatments resulted in differing levels of degradation.

Figure 9:

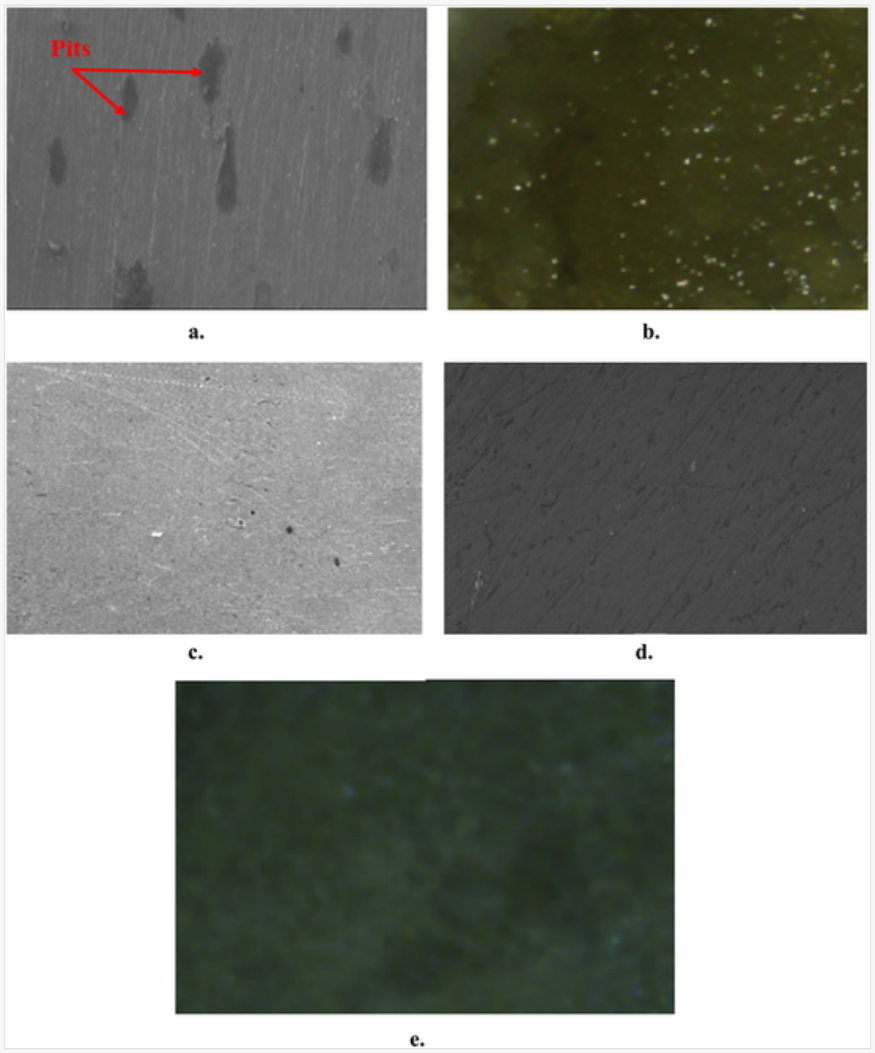

Fig.9. Microstructural Morphology analyis, (a) Cast iron (b) Cast iron (gel) (c) Stainless steel (d) Mild steel (e) Mild steel (gel) surface morphology of specimen after corrosion at 1,000x magnification.

As can be seen in Figure 9(a), cast iron exhibits severe corrosion characterized by deep and uniform pits with the depth of 5 mm. Corrosion in cast iron is known to be due to the presence of graphite flakes which serve as anodic and cathodic sites that cause localized attack leading to loss of the material and surface roughness. In contrast, Gel-treated cast iron is shown in Figure 9(b) as the protective coating serves as a barrier against moisture and oxygen, considerably reducing the formation of pits and improving corrosion resistance. The best protection comes from stainless steel which forms a protective chromium oxide layer preventing large areas of damage, although some small pitting corrosion is still observed in aggressive environments with the presence of chlorides, as illustrated in Figure 9(c). On the other hand, as seen in Figure 9(d), the mild steel experience severe corrosion, especially known to be caused by the absence of inclusions of corrosion-resistant alloys, thus prone to oxidation and rust generation. However, a gel coat application, similar to that shown in Figure 9(e) can reduce surface defects and delay the process of oxidation, thus severely mitigating the corrosion

effects on mild steel. The findings highlight those protective treatments are key to improving the corrosion resistance of metals, with stainless steel having the highest level of natural resistance and untreated mild steel and cast iron being the most corrosion-prone.

4 Conclusions

This study presents a critical review of reported corrosion rates of cast iron, mild steel, and stainless steel in the biodiesel being studied, across the exposure period of 1,872 h at ambient temperature. The results clearly indicate that stainless steel has the highest resistance toward corrosion when compared with other metals. More specifically the recorded corrosion rates were 0.0173 mm/year (diesel); 0.0178 mm/year (Jatropha biodiesel); and 0.0194 mm/year Karanja biodiesel. The results show that stainless steel greatly surpasses the other materials in the immersion time indicated regarding the corrosion of biodiesel. On the other hand, cast iron shows high rates of corrosion, especially with Karanja biodiesel, of 0.0528 mm/year. In diesel, cast iron still has a high corrosion rate of 0.0505 mm/year. This significant difference illustrates the susceptibility of domestic cast iron towards corrosive environments, perhaps because of its chemical reactivity with biodiesel. Also, findings showed that the rate of corrosion of the stainless steel decreased as hydration time in the same solution increased, which could indicate that a protective behaviour arises during prolonged exposure.

The physical state of the metal specimens after the immersion period had stark differences visually. After exposure cast iron and mild steel was covered in a yellowish, sticky gel like material, which does not happen with stainless steel which also remained largely unaffected. These formations are particularly alarming because they can rob fuel lines and hinder engine functioning, essentially endangering the operators. These observations were verified through advanced surface morphology analysis. The grinding lines were visibly clear for all stainless-steel samples at 1,000x, suggesting little or no degradation. In contrast, on the other hand, the faces of cast iron and mild steel experienced extensive modifications, including an attack where uniform pits with residence of approximately 5 mm were created. This change in surface architecture not only suggests that material degradation takes place, but also highlights the need for careful selection of materials in biodiesel exposure situations. This study is indicative of the importance of material selection for biodiesel usage. The other options have less resistance to corrosion than stainless steel, and mild and cast iron are not as structurally stable. But as biodiesel emerges as a realistic replacement fuel across the automotive and industrial arena, working out the “how’s” of material compatibility and, at least, corrosion performance will be the key to providing long-term stability in fuel systems.

5 Future scope of work

i. The impact of different biodiesel blends on material degradation under various operating conditions, including long-term exposure at elevated temperatures.

ii. Exploration of novel corrosion inhibitors or additives that can be incorporated into biodiesel to reduce its corrosive effect on metals.

iii. The selection and development of materials that are resistant to corrosion in biodiesel systems, particularly for long-term storage and transportation.

iv. The use of advanced coatings or protective treatments to mitigate corrosion and enhance the durability of storage tanks, pipelines, and other infrastructure.

v. Future investigations may consider additional materials to determine suitability in biodiesel infrastructure.

6 Limitations of study

i. The study address corrosion behavior, and does not address other important properties associated with biodiesel blends, such as fuel economy, emissions, or engine performance.

ii. This study assumes a homogeneity of biodiesel composition, while in fact, the composition can vary accordingly to the feedstock, production methods and storage conditions

iii. The corrosion behaviour reported in this study is based on laboratory immersion tests, which might not completely represent the conditions present in complex real biodiesel storage and transportation systems.

Acknowledgments

~~This research work has received no funding.~~The authors extend their appreciation to the Deanship of Scientific Research at King Khalid University for funding this work through large group Research Project under grant number RGP2/28/44.

References

The corrections made in this section will be reviewed by journal production editor.

[1] P. T. Vasudevan and M. Briggs, “Biodiesel production – current state of the art and challenges,” *J. Ind. Microbiol. Biotechnol.*, vol. 35, no. 5, pp. 421–430, 2008. https://doi.org/10.1007/s10295-008-0312-2.

Q9 [2] D. Chandran, “Compatibility of diesel engine materials with biodiesel fuel,” *Renewable energy*, vol. 147, pp. 89–99, 2020. https://doi.org/10.1016/j.renene.2019.08.040.

[3] T. Mizik and G. Gyarmati, “Economic and sustainability of biodiesel production – a systematic literature review,” *Clean Technol.*, vol. 3, no. 1, pp. 19–36, 2021. https://doi.org/10.3390/cleantechnol3010002.

[4] M. Takase, et al., “An expatiate review of neem, jatropha, rubber and karanja as multipurpose non-edible biodiesel resources and comparison of their fuel, engine and emission properties,” *Renewable Sustainable Energy Rev.*, vol. 43, pp. 495–520, 2015. https://doi.org/10.1016/j.rser.2014.11.049.

[5] Z. Zhang, et al., “Utilization of hydrogen-diesel blends for the improvements of a dual-fuel engine based on the improved Taguchi methodology,” *Energy*, vol. 292, p. 130474, 2024. https://doi.org/10.1016/j.energy.2024.130474.

[6] P. Adewale, M.-J. Dumont, and M. Ngadi, “Recent trends of biodiesel production from animal fat wastes and associated production techniques,” *Renewable Sustainable Energy Rev.*, vol. 45, pp. 574–588, 2015. https://doi.org/10.1016/j.rser.2015.02.039.

[7] G. Corro, N. Sánchez, U. Pal, and F. Bañuelos, “Biodiesel production from waste frying oil using waste animal bone and solar heat,” *Waste Manage.*, pp. 1–9, 2015. https://doi.org/10.1016/j.wasman.2015.02.00.

[8] T. K. Jose and K. Anand, “Effects of biodiesel composition on its long term storage stability,” *Fuel*, vol. 177, pp. 190–196, 2016. https://doi.org/10.1016/j.fuel.2016.03.007.

[9] P. Bennett, “Rust: an age old problem,” *Mater. Today*, vol. 30, pp. 103–104, 2019. https://doi.org/10.1016/j.mattod.2019.09.019.

[10] S. M. Alves, F. K. Dutra-Pereira, and T. D. C. Bicudo, “Influence of stainless steel corrosion on biodiesel oxidative stability during storage,” *Fuel*, vol. 249, pp. 73–79, 2019. https://doi.org/10.1016/j.fuel.2019.03.097.

[11] F. V. Adams, A. T. Bankole, O. P. Sylvester, A. O. Apata, I. V. Joseph, and O. M. Ama, “Corrosion behavior of ferritic stainless steel in locally prepared biodiesel media,” in *Proceedings of the World Congress on Engineering WCE. II*, London, WCE, 2018.

[12] L. N. Komariah, S. Arita, B. E. Prianda, and T. K. Dewi, “Technical assessment of biodiesel storage tank; a corrosion case study,” *J. King Saud Univ.-Eng. Sci.*, vol. 35, no. 3, pp. 232–237, 2023. https://doi.org/10.1016/j.jksues.2021.03.016.

[13] M. A. Fazal, A. Haseeb, and H. Masjuki, “Effect of temperature on the corrosion behavior of mild steel upon exposure to palm biodiesel,” *Energy*, vol. 36, no. 5, pp. 3328–3334, 2011. https://doi.org/10.1016/j.energy.2011.03.028.

[14] K. V. Chew, A. S. M. A. Haseeb, H. H. Masjuki, M. A. Fazal, and M. Gupta, “Corrosion of magnesium and aluminum in palm biodiesel: a comparative evaluation,” *Energy*, vol. 57, pp. 478–483, 2013. https://doi.org/10.1016/j.energy.2013.04.067.

[15] D. Jin, X. Zhou, P. Wu, L. Jiang, and H. Ge, “Corrosion behavior of ASTM 1045 mild steel in palm biodiesel,” *Renewable Energy*, vol. 81, pp. 457–463, 2015. https://doi.org/10.1016/j.renene.2015.03.022.

[16] A. E. Sterpu, B. G. Simedrea, T. V. Chis, and O. V. Săpunaru, “Corrosion effect of biodiesel-diesel blend on different metals/alloy as automotive components materials,” *Fuels*, vol. 5, no. 1, pp. 17–32, 2024. https://doi.org/10.3390/fuels5010002.

[17] B. Singh, J. Korstad, and Y. C. Sharma, “A critical review on corrosion of compression ignition (CI) engine parts by biodiesel and biodiesel blends and its inhibition,” *Renewable Sustainable Energy Rev.*, vol. 16, no. 5, pp. 3401–3408, 2012. https://doi.org/10.1016/j.rser.2012.02.042.

[18] A. S. Román, C. M. Méndez, and A. E. Ares, “Corrosion resistance of stainless steels in biodiesel,” in *Shape Casting: 6th International Symposium*, Hoboken, NJ, USA, John Wiley & Sons, Inc., 2016, pp. 109–116.

[19] S. M. Alves, F. K. Dutra-Pereira, and T. D. C. Bicudo, “Influence of stainless steel corrosion on biodiesel oxidative stability during storage,” *Fuel*, vol. 249, pp. 73–79, 2019. https://doi.org/10.1016/j.fuel.2019.03.097.

[20] N. Kumar, “Oxidative stability of biodiesel: causes, effects and prevention,” *Fuel*, vol. 190, no. 15 February 2017, pp. 328–350, 2017. https://doi.org/10.1016/j.fuel.2016.11.001.

[21] L. M. Baena, F. Vásquez, and J. A. Calderón, “Corrosion assessment of metals in bioethanol-gasoline blends using electrochemical impedance spectroscopy,” *Heliyon*, vol. 7, no. 7, p. 07585, 2021. https://doi.org/10.1016/j.heliyon.2021.e07585.

[22] C.L. Kugelmeier, M.R. Monteiro, R. da Silva, S.E. Kuri, V.L. Sordi, and C.A. Della Rovere, “Corrosion behavior of carbon steel, stainless steel, aluminum and copper upon exposure to biodiesel blended with petrodiesel,” *Energy*, vol. 226, p. 120344, 2021. https://doi.org/10.1016/j.energy.2021.120344.

[23] F. Sundus, M. Fazal, and H. Masjuki, “Tribology with biodiesel: a study on enhancing biodiesel stability and its fuel properties,” *Renew. Sustain. Energy Rev.*, vol. 70, pp. 399–412, 2017. https://doi.org/10.1016/j.rser.2016.11.217.

[24] J. Goellner, A. Burkert, A. Heyn, E. Boese, O. Ezers’ ka, and J. Hickling, “State-of-the-art of corrosion testing by using electrochemical noise measurements,” *Mater. Sci.*, vol. 37, no. 3, pp. 509–519, 2001. Available at: https://doi.org/10.1023/a:1013222525386.

[25] S Kanchan, et al., “Developing a model for waste plastic biofuels in CRDi diesel engines using FTIR, GCMS, and WASPAS synchronisations for engine analysis,” *Energy Explor. Exploit.*, vol. 0, no. 0, 2023. https://doi.org/10.1177/01445987231216762.

Footnotes

Text Footnotes

Research ethics: Not applicable.

Author contributions: Conceptualization, Maninder Singh (MS), Mukhtiar Singh (MS), HS, MSR, AS, RK, SS; formal analysis, Maninder Singh (MS), Mukhtiar Singh (MS), HS, MSR, AS, RK, SS; investigation, Maninder Singh (MS), Mukhtiar Singh (MS), HS, MSR, AS, RK, SS; writing – original draft preparation, Maninder Singh (MS), Mukhtiar Singh (MS), HS, MSR, AS, RK, SS; writing – review and editing, SS, VNR, PK, RD, RS, AK; supervision, SS, VNR, PK, RD, RS, AK; project administration, SS, VNR, PK, RD, RS, AK; funding acquisition, SS, VNR, PK, RD, RS, AK. All authors have read and agreed to the published version of the manuscript.

Conflict of interest: The authors declare no competing interests.

Research funding: ~~This research work has received no funding.~~ The authors extend their appreciation to the Deanship of Scientific Research at King Khalid University for funding this work through large group Research Project under grant number RGP2/28/44.

Data availabilQ8**:** ~~My manuscript has no associate data.~~ All the data and related findings that has been used throughout this manuscript are available from the co-authors, Maninder Singh and Rajeev Kumar. Both are responsible for providing the findings and datasets that has been used in this work.

Supplementary Material

j_ijcre-2024-0205_suppl_001.pdf

Supplementary Material

This article contains supplementary material (https://doi.org/10.1515/ijcre-2024-0205).

Queries and Answers

Q1

Query: Please note that the short title will be used as running head on top of the pages. Please check the retained short title or kindly provide the short title fewer than 75 characters including space.

Answer: KINDLY RETAIN THE SAME.

Q2

Query: As per De Gruyter policy, no author list changes are permitted after acceptance of an article. The De Gruyter production team is instructed to enforce this policy during the production/proofing process.

Answer: KINDLY CONSIDER THE CHANGES MADE IN THE AUTHOR'S AFFILIATION DURING THE FINAL ONLINE PUBLICATION AND PRODUCTION OF THE ARTICLE.

Q3

Query: Please confirm that the forename(s) and surname(s) have been identified correctly and please carefully verify the spelling of all authors' names.

Answer: I CONFIRM THE SAME.

Q4

Query: Please note that as per the journal style, only one email address should be included for the corresponding author. Kindly check and advise on the one to be retained.

Answer: Kindly consider the following mail,

shubhamsharma914819149vdvn@gmail.com

Q5

Query: Please provide the city name for the affiliation 5.

Answer: The city name is Irbid.

Q6

Query: Reference 28 is cited in the text but not provided in the reference list. Please provide it in the reference list or alternatively delete the citations from the text.

Answer: The reference [28] has been deleted now.

Q7

Query: Please provide the main caption for the figures 3 and 9.

Answer: Modified

Q8

Query: Please note that we have received the Template for Ethical and Legal Declarations for author statements for this item without the headings "Informed consent, Use of Large Language Models, AI and Machine Learning Tools" Please check and provide the missing headings following style. You can download the template here: https://degruyter.knack.com/joda-20#template-for-ethical-and-legal-declarations/.

Answer: Informed consent: Not Applicable

Use of Large Language Models, AI and Machine Learning Tools: Not Applicable

Q9

Query: Please provide the issue number for the references 2, 4, 5, 6, 7, 8, 9, 10, 14, 15, 19, 22, 23.

Answer: Reference 2: Issue no. 1

Reference 4: Issue no. 0

Reference 5: Issue no. 0

Reference 6: Issue no. 0

Reference 7: Issue no. 0

Reference 8: Issue no. 0

Reference 9: Issue no. 0

Reference 10: Issue no. 0

Reference 14: Issue no. 0

Reference 15: Issue no. 0

Reference 19: Issue no. 0

Reference 22: Issue no. 0

Reference 23: Issue no. 0